Volume 14 | Number 26 | 14 July 2018 | Pages 5335–5538

Soft Matter

rsc.li/soft-matter-journal

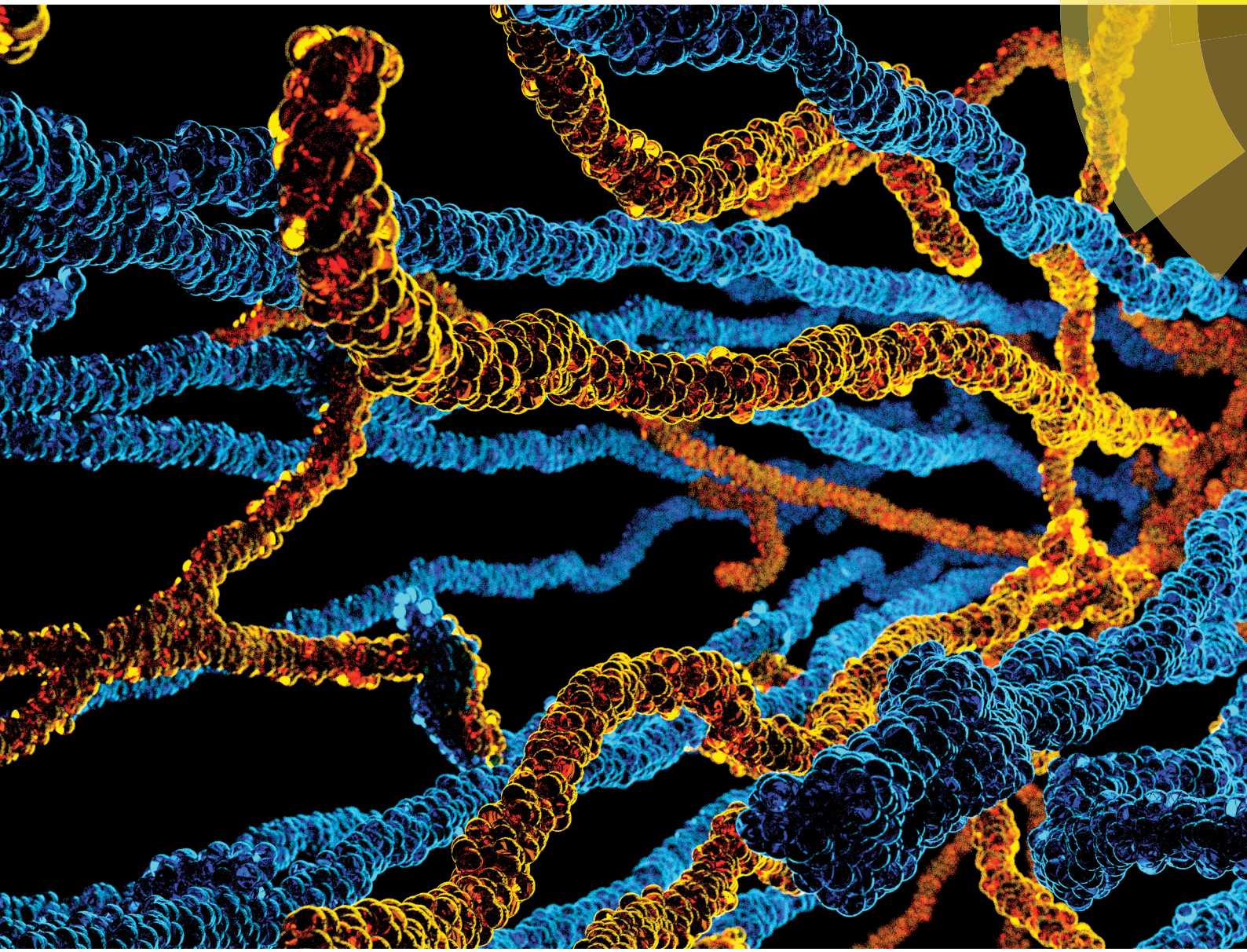

ISSN 1744-6848

ROYAL SOCIETY OF CHEMISTRY

PAPER

Paul D. Butler *et al.*

Branching and alignment in reverse worm-like micelles studied with simultaneous dielectric spectroscopy and RheoSANS

Soft Matter

PAPER

View Article Online
View Journal | View Issue

Cite this: *Soft Matter*, 2018, **14**, 5344

Branching and alignment in reverse worm-like micelles studied with simultaneous dielectric spectroscopy and RheoSANS†

John K. Riley, [a] Jeffrey J. Richards, [a] Norman J. Wagner [b] and Paul D. Butler*[a]

Topology and branching play an important but poorly understood role in controlling the mechanical and flow properties of worm-like micelles (WLMs). To address the challenge of characterizing branching during flow of WLMs, dielectric spectroscopy, rheology, and small-angle neutron scattering (dielectric RheoSANS) experiments are performed simultaneously to measure the concurrent evolution of conductivity, permittivity, stress, and segmental anisotropy of reverse WLMs under steady-shear flow. Reverse WLMs are microemulsions comprised of the phospholipid surfactant lecithin dispersed in oil with water solubilized in the micelle core. Their electrical properties are independently sensitive to the WLM topology and dynamics. To isolate the effects of branching, dielectric RheoSANS is performed on WLMs in *n*-decane, which show fast breakage times and exhibit a continuous branching transition for water-to-surfactant ratios above the corresponding maximum in zero-shear viscosity. The unbranched WLMs in *n*-decane exhibit only subtle decreases in their electrical properties under flow that are driven by chain alignment and structural anisotropy in the plane perpendicular to the electric field and incident neutron beam. These results are in qualitative agreement with additional measurements on a purely linear WLM system in cyclohexane despite differences in breakage kinetics and a stronger tendency for the latter to shear band. In contrast, the branched micelles in *n*-decane (higher water content) undergo non-monotonic changes in permittivity and more pronounced decreases in conductivity under flow. The combined steady-shear electrical and microstructural measurements are capable, for the first time, of resolving branch breaking at low shear rates prior to alignment-driven anisotropy at higher shear rates.

Received 13th April 2018,
Accepted 17th May 2018

DOI: 10.1039/c8sm00770e

rsc.li/soft-matter-journal

Introduction

Surfactant self-assembly into worm-like or polymer-like micelles (WLM/PLM)[1] is widely studied as a practical method for modifying the viscoelastic properties of both aqueous[2] and non-aqueous[3] complex fluid formulations. The tendency of WLMs to break and reform, entangle and reptate, and form branched topologies gives rise to both a rich microstructural behavior in response to deformation[4,5] and a complicated flow phenomena such as shear banding[6] and shear-induced phase separation.[7] These complexities have challenged researchers to develop theoretical models[5,8,9] and experimental techniques[10–12] necessary to determine and describe structure–property relationships for WLMs.

In particular, micellar topology plays a critical but poorly understood role in governing the flow properties of WLMs.[13] A transition from linear to branched topology occurs as the endcap or scission energy of the micelles increases relative to the energy for branch formation. Instead of breaking into shorter micelles to generate endcaps, WLMs tend to fuse and form three-fold junctions between worm-like chains.[14] The onset of branching and evolution of WLMs from a linear and entangled solution to a branched and connected network is identified by a maximum in zero-shear viscosity that most WLM systems exhibit as a function of the micelle growth variable. The relationship between topology and a decrease in viscosity is rationalized with the idea that branch points along a WLM chain backbone are fluid and that sliding of these branch points can relieve stress when WLMs flow.[15] The most convincing observations of these topologies have been conducted with cryo-TEM.[16] Imaging of linear or branched WLMs *via* cryo-TEM tends to be consistent with the evolution of rheological properties below and above the viscosity maximum. The major disadvantage of electron microscopy is that it cannot be applied during flow of

[a] *Center for Neutron Research, National Institute of Standards and Technology, Gaithersburg, MD, 20899-6100, USA. E-mail: paul.butler@nist.gov*
[b] *Center for Neutron Science, Department of Chemical and Biomolecular Engineering, University of Delaware, Newark, DE, 19716, USA*

† Electronic supplementary information (ESI) available: Full dielectric spectra, representative 2D and 1D SANS patterns, relevant sample information. See DOI: 10.1039/c8sm00770e

the WLMs, which is relevant for processing and necessary to reveal underlying constitutive relationships between deformation and shear stress. Recent scattering models have been developed which account for branching in dilute WLMs,[17] but it is unclear if these models perform well at describing concentrated and entangled WLMs solutions.

Further challenges arise when attempting to isolate linear-to-branched transitions in the widely studied aqueous WLM systems comprised of ionic surfactants. In such systems, branching is induced with the addition of salt which screens electrostatic repulsions between headgroups; however, this has the coupled effect of changing the end-cap energy and thus the topology, changing the local surfactant ordering or persistence length of the WLMs,[18] and changing the strength of inter-micellar electrostatic repulsions. The latter is important when studying semi-dilute or concentrated WLM solutions *via* rheology or scattering. One example is a recent RheoSANS study of branching effects on the flow of aqueous CTAT/SDBS WLMs.[19] Here, the hydrotropic salt sodium tosylate was added to induce branching, which strongly influenced the segmental electrostatic interactions as evidenced by the presence of a strong structure factor peak in the scattering at low salt concentrations which disappears at higher salt concentrations where branches form. Screening of the electrostatic repulsions dominates the primary rheological relaxation time and contributes to the differences in steady-shear flow behavior. These coupled changes in topology, local structure, and interactions plague many aqueous ionic surfactant systems, making them generally ill-suited for specifically isolating topological effects during flow of WLMs with traditional rheological and scattering techniques.

To address the challenge of (1) measuring branching *in situ* during flow and (2) avoiding strong electrostatic interactions that convolute with structural and topological transitions, we choose to study reverse WLMs that form in non-polar solvents.[3] One such classical reverse WLM system is comprised of the phospholipid surfactant, lecithin, dissolved in oil. Upon the addition of small amounts of water, lecithin reverse micelles ($\sim$5 nm diameter spheres) grow into reverse WLMs ($\approx$μm in length, $\approx$5 nm in diameter) as water is solubilized in the core by the hydrophilic lipid headgroups.[20] Lecithin is an important and abundant amphiphilic lipid derived from crude plant (*e.g.* soy) and animal (*e.g.* egg yolk) oil sources and used broadly as a surfactant and rheology modifier in food products. The structure and rheological properties of lecithin reverse WLMs have been thoroughly characterized *via* neutron[21,22] and light[22,23] scattering, rheology,[24–26] and flow/rheo-SANS[27–29] techniques.

Lecithin reverse WLMs have the benefit of being thermodynamically stable water-in-oil microemulsions,[30] and the strong dielectric contrast between the oil and water phases in these systems provides exquisite sensitivity to changes in microemulsion shape, size, orientation,[31] and connectivity *via* percolation of aqueous domains.[32,33] Leveraging this sensitivity, Cirkel and co-workers used AC dielectric spectroscopy to identify the presence of branching in lecithin/water/isooctane reverse WLMs.[34] They characterized the system in terms of a low-frequency conductivity and two-distinct dielectric relaxations in the permittivity spectra. The scaling of low-frequency conductivity with micelle concentration could only be explained by branching and the formation of interconnected and percolated water networks. The low-frequency relaxation (1 to 1000 Hz) observed in the permittivity spectra reflected segmental dynamics which change as the micelles grow and entangle. The ability to simultaneously probe micelle connectivity and chain mobility with a non-invasive technique makes dielectric spectroscopy ideally suited for studying the properties of reverse WLMs under flow.

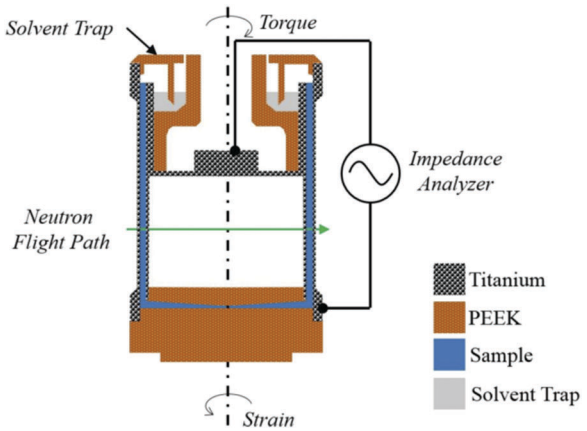

Fig. 1 Cross-section of the dielectric RheoSANS Couette cell for use in a commercial strain-controlled rheometer. Reproduced with permission from ref. 36.

In this work, we expand such dielectric spectroscopy analysis to both lecithin-based reverse WLMs undergoing steady-shear flow using the newly developed method of dielectric RheoSANS,[35,36] depicted schematically in Fig. 1. This technique allows us to concurrently measure stress, complex impedance, and small-angle neutron scattering (SANS) of the WLMs in a strain-controlled rheometer at prescribed shear rates. The complex impedance spectra are converted to AC permittivity and conductivity which are used to evaluate changes in branching and micelle dynamics under flow. The 2D SANS patterns are used to track segmental alignment in the flow-vorticity plane of shear. Dielectric RheoSANS experiments are performed for WLMs in decane at compositions where the micelles are branched and unbranched, and complimented with measurements on a second purely linear WLM system in cyclohexane.

Materials and methods

Materials

Deuterated *n*-decane (d_{22}, 97% purity) was purchased from Cambridge Isotopes Laboratories Inc. and used as received. Soy Lecithin (95% purity) was purchased from Avanti Polar Lipids and contains a distribution of lipid tail lengths resulting in an average lipid molecular weight of 775.04 g mol^{-1}. The lipid tail distribution provided by the manufacturer is shown in the ESI.† Growth of the micelles into elongated, flexible worm-like chains is controlled by the molar ratio of water to surfactant, $W = [H_2O]/[Lec]$. Lecithin as received is hygroscopic and contains

bound water. Given the sensitivity of micelle growth to water content, care was taken to consistently "dry" the lipid prior to preparation of reverse WLMs. Thus, lipid was first fully dissolved in methanol to produce a reddish solution. The methanol was evaporated off overnight by gently passing a stream of nitrogen over the solution in a fume hood, producing a viscous lipid gel. The remaining lipid was placed in a vacuum oven and dried for 48 hours at ambient temperature to produce a gummy solid. Upon removal from the vacuum oven the container was back-filled with nitrogen, sealed, and stored in the dark until use. Reverse WLMs were prepared by dissolving the appropriate amount of "dry" lipid in oil to produce a Newtonian solution of reverse micelles. An appropriate ratio of this dry surfactant solution in oil and de-ionized water were added to a well-sealed glass vial and gently agitated overnight on a roll mixer. This preparation produced transparent, homogeneous, viscoelastic WLM solutions. The WLMs were equilibrated at ambient temperature for at least 24 hours prior to experiments.

Dielectric RheoSANS

The instrument used to perform dielectric RheoSANS experiments (Fig. 1) has been detailed previously in the literature.[35,36] Briefly, an ARES-G2 strain-controlled rheometer (TA Instruments, New Castle, DE) is fit with a modified forced-convection oven that allows access for neutrons to illuminate a titanium Couette geometry for RheoSANS measurements in the flow-vorticity ("1–3") plane. The titanium cup and bob provide suitable neutron transmission and also serve as the two electrodes for AC dielectric spectroscopy,[37] which is performed using an LCR meter (E4890A, Keysight Technologies, Santa Rosa, CA) over a frequency range of f = 20 Hz to 2 MHz. The dielectric spectra are analyzed both in terms of the AC conductivity $\sigma(f)$ and permittivity $\varepsilon_{app}'(f)$ obtained from the measured complex impedance $Z^*(f)$ after open and short circuit compensations: $Y^*(f) = 1/Z^*(f) = C[\sigma(f) + i\omega\varepsilon_0\varepsilon_{app}'(f)]$, where the cell constant C is determined by calibrating against KCl conductivity standards. Similarly, we can represent the same dielectric spectra using the general formalism of a complex permittivity $\varepsilon^*(f) = Y^*/2\pi fC\varepsilon_0 = \varepsilon' - i\varepsilon''$ consisting of an in-phase dielectric storage ε' and out-of-phase dielectric loss ε'' component. From this, we can define the dielectric loss tangent $\tan\delta_e = \varepsilon''/\varepsilon'$ which gives a measure of the ratio of resistive and capacitive processes and is useful for visually identifying distinct dielectric relaxation phenomena, which appear as peaks in the spectra.

SANS measurements are carried out on the NG-7 30 m small angle neutron scattering instrument[38] at the NIST Center for Neutron Research at the National Institute of Standards and Technology in Gaithersburg, MD. SANS profiles were collected at three configurations to cover a Q-range from 0.001 Å^{-1} to 0.1 Å^{-1}, where $Q = 4\pi/\lambda \sin\theta$, λ being the neutron wavelength and 2θ the total scattering angle. All three configurations were taken at λ = 6 Å with $\Delta\lambda/\lambda$ = 14%. After accounting for transmission, background, empty cell scattering, and detector efficiency, the data were reduced to absolute scale using the standard NCNR reduction macros in Igor Pro.[39] All experiments are performed at a temperature of (25 ± 0.5 °C). RheoSANS measurements were performed in the flow-vorticity (1–3) plane of shear, where alignment of segments in the flow direction leads to anisotropy in the scattering patterns. The degree of anisotropy at a length scale corresponding to the persistence length of the WLMs is quantified *via* an alignment factor, A_f, which is a scalar value calculated from the annular average of the 2D scattering intensity $I(q,\phi)$ evaluated around a central scattering vector q^*.[40]

$$A_f = \frac{\int_0^{2\pi} I(q^*,\phi)\cos(2\phi)\mathrm{d}\phi}{\int_0^{2\pi} I(q^*,\phi)\mathrm{d}\phi} \quad \text{(S1)}$$

The alignment factor varies from 0 for isotropic scattering to 1 for full alignment. Representative annular and circular average 1D SANS profiles are provided in the ESI.†

Results and discussion

Topological distinction between reverse WLMs at rest and under flow

The primary objective of this work is to measure the rheological, electrical, and microstructural properties of unbranched and branched WLMs in *n*-decane. The topology of similar lecithin WLM systems in isooctane has been established previously based on dielectric characterization[34,41] and PGSE-NMR measurements of water diffusion through the micelle core.[42] The ternary phase behavior of lecithin/water/decane and lecithin/water/isooctane have been shown to be nearly indistinguishable.[30] The linear viscoelastic properties of WLMs are also commonly used to demonstrate growth and topological transitions. A maximum in zero-shear viscosity (η_0) corresponds to compositions where the micelles are longest and exhibit the strongest entanglement. Fig. 2 shows a growth curve for lecithin WLMs in hydrogenated decane as a function of added water measured by rotational rheology. A zero-shear viscosity maximum in *n*-decane is observed at W_{max} = 2.5, above which the viscosity drops as branches form followed by phase separation near W_{PS} = 3.0. The absolute value of W depends on the lecithin purity, composition, and drying procedure, and thus can differ between reports in the literature and even preparation. Phase separation occurs when the number of branch points approaches the number of WLM segments,[43] and in the reverse WLM system results in the expulsion of oil into an upper phase and separation of a lower concentrated lower gel phase. The "branched WLM" samples are prepared in deuterated *n*-decane at W = 2.8 just below the phase separation boundary and the "unbranched WLM" sample in deuterated *n*-decane is prepared at W = 2.4 just below the zero-shear viscosity maximum. Small-amplitude oscillatory shear rheology on the branched and unbranched WLMs is also shown in Fig. 2. The viscoelasticity of the decane WLMs deviates slightly from pure Maxwellian behavior but is still be well-described by a single characteristic relaxation time and a rubbery plateau. The rheological relaxation time is determined from the crossover frequency $\tau_R = 1/\omega_c$ and the plateau modulus G_p from the value of the storage modulus G' at a frequency corresponding to the minimum in loss modulus G''. The unbranched WLMs have τ_R = 2.5 s and G_p = 38 Pa and the branched

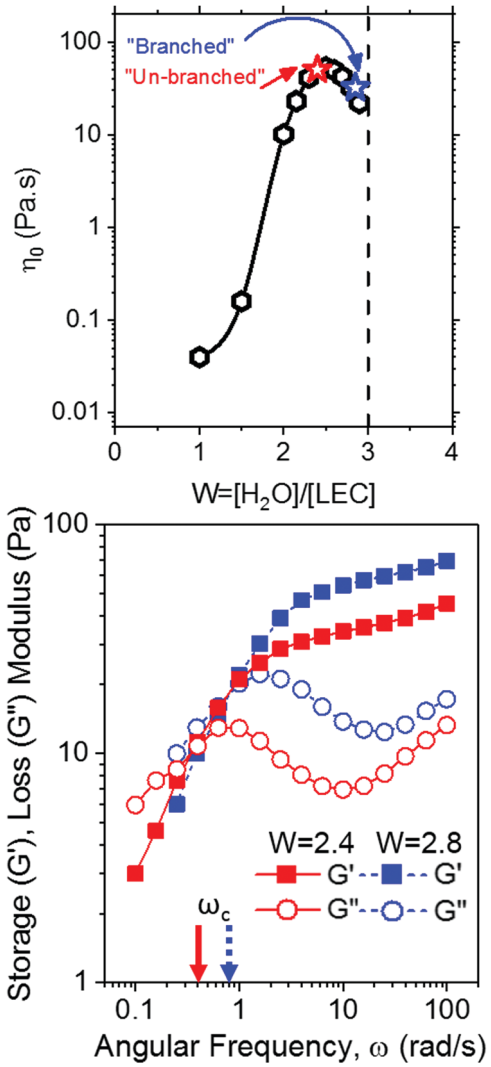

Fig. 2 Linear viscoelastic properties of reverse WLMs in *n*-decane at a lecithin concentration of 50 mg mL^{-1} as a function of the molar ratio of water to surfactant, *W*. (top) WLM growth curve showing the evolution of zero-shear viscosity in hydrogenated decane (open hexagons). Stars indicate the compositions for branched and un-branched WLMs in deuterated decane to be probed *via* dielectric RheoSANS. (bottom) Small-amplitude oscillatory shear rheology of reverse WLMs in deuterated decane at a strain amplitude of 0.5%. The crossover frequencies are indicated by the arrows on the *x*-axis.

WLMs have τ_R = 1.25 s and G_p = 60 Pa. The subtle effect of branching on the linear viscoelastic properties is representative of the continuous unbranched-to-branched transition that occurs in these systems independent of strong changes in intermicellar interactions.

Dielectric spectroscopy provides an additional method for characterizing topology in reverse WLMs. The scaling of the conductivity with micelle concentration and water content provided initial evidence for branching in lecithin reverse micelles.[34] Quiescent dielectric frequency sweeps were performed here on the branched and unbranched WLMs in decane and the low-frequency region of the conductivity spectra is shown in Fig. 3. The conductivity of linear WLMs in cyclohexane is also included for comparison. The lecithin/water/cyclohexane WLMs are unique in that they have a strong preference to form purely linear WLMs and do not form branched topologies. Instead of branching these micelles undergo a cylinder-to-sphere transition above the zero-shear viscosity maximum.[44,45] Because of the very large end-cap energy in the cyclohexane WLMs their corresponding breakage times are very slow,[26] resulting in a system that mimics "dead polymers". Measured breakup times for cyclohexane WLMs (≈minutes) are orders of magnitude slower than the breakage times reported for WLMs that obey traditional linear-to-branched topological transitions and have fast breakage kinetics (≈0.1 s) when entangled.[46] This has important implications on the non-linear rheology of the cyclohexane WLMs to be discussed later.

Static dielectric spectroscopy reveals differences in low-frequency conductivity between linear micelles in cyclohexane, unbranched micelles in decane, and branched micelles in decane, as shown in Fig. 3. The branched WLMs display a low-frequency conductivity plateau in the quiescent state that increases as micelle concentration is increased from 50 mg mL^{-1} to 75 mg mL^{-1}. The unbranched WLMs in decane also have a low-frequency conductivity plateau much like the branched micelles, but whose magnitude is significantly smaller. Interestingly, the unbranched micelles display AC behavior more like the branched WLMs than the linear WLMs in cyclohexane. The low-frequency conductivity plateau present for both the branched and unbranched systems in decane is absent from the dielectric spectra of the disconnected, linear micelles over this frequency range. A frequency-independent conductivity is suggestive of a DC-conductivity, which is a measure of charge transport across the gap in our experimental setup. The conductivity plateau for the cyclohexane WLMs appears to be outside of our resolvable frequency range, indicating that it has a value much lower than is measured here for the decane WLMs. This is striking considering the cyclohexane WLMs are prepared at W = 10, thus having approximately 3.6 times more water solubilized than the decane WLMs at an equivalent lecithin concentration of 75 mg mL^{-1}.

Our data suggests that topology alone cannot describe the differences in conductivity between the three WLMs compared herein. Charge conduction in these systems must occur

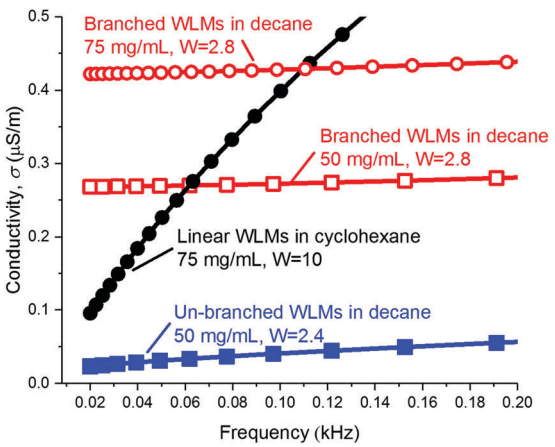

Fig. 3 Low-frequency region of AC conductivity spectra for reverse WLMs at rest.

through the water-rich micelle cores and therefore the dynamic micelle breakage and reformation must play a prominent role in the transport of ions between micelles and across the gap. This is manifested in the frequency-dependence of the conductivity. Thus, the strong tendency of WLMs in cyclohexane to resist break-up hinders ion transport between micelles and contributes to the extremely low conductivity plateau that lies outside of our measurement window. Topology also plays a role in that it contributes to the magnitude of the conductivity plateau. As evidenced by the electrical properties, the differences in self-assembly behavior in decane and cyclohexane are critical and must be emphasized strongly to avoid confusion in terminology: "Linear WLMs" in cyclohexane are in fact purely linear and have slow breakage times while "unbranched WLMs" in decane have faster breakage and recombination dynamics and are not explicitly linear, but topology is limited to localized intramicellar junctions rather than the large-scale percolated pathways present in the branched system.

Further insight into the topology of linear and branched WLMs can be made by inspection of the dielectric loss tangent both at rest and under shear, as is done in Fig. 4. The dielectric loss tangents are again presented for linear WLMs in cyclohexane, branched WLMs in decane, and unbranched WLMs in decane in response to flow. The first major difference arises between the cyclohexane WLMs and the decane WLMs. In cyclohexane the WLMs exhibit a single, broad dielectric relaxation that is weakly sensitive to shear over the measured range of frequencies. In decane, the WLMs exhibit two distinct regions of dielectric relaxation: a high-frequency (HF) (>100 kHz) relaxation and a series of low-frequency (LF) relaxations (<50 kHz). The ability to resolve the high-frequency relaxation appears tied to the water concentration in the system. The molar ratio of water to surfactant is $W = 10$ for the WLMs in cyclohexane and varies between $W = 2.4$ and $W = 2.8$ for the WLMs in decane. In decane, the position of the local minimum that separates the LF and HF regions shifts to higher frequency as W increases. It is logical then that in cyclohexane, where $W = 10$, the HF relaxation appears to shift out of our measurable frequency range. This suggests that the HF relaxation is tied to interfacial polarization that arises at the oil/surfactant/water interface due to the dielectric contrast between the solvent/lecithin tails and the micelle core comprised of water and the lecithin headgroups. Importantly, this HF relaxation appears to be de-coupled from the LF relaxation in the case of the branched WLMs in decane.

A second major difference arises when comparing the relative strengths of the dielectric loss tangents. The purely linear micelles in cyclohexane and the unbranched micelles in decane display $\tan\delta_e \leq 1$ across the entire frequency range.

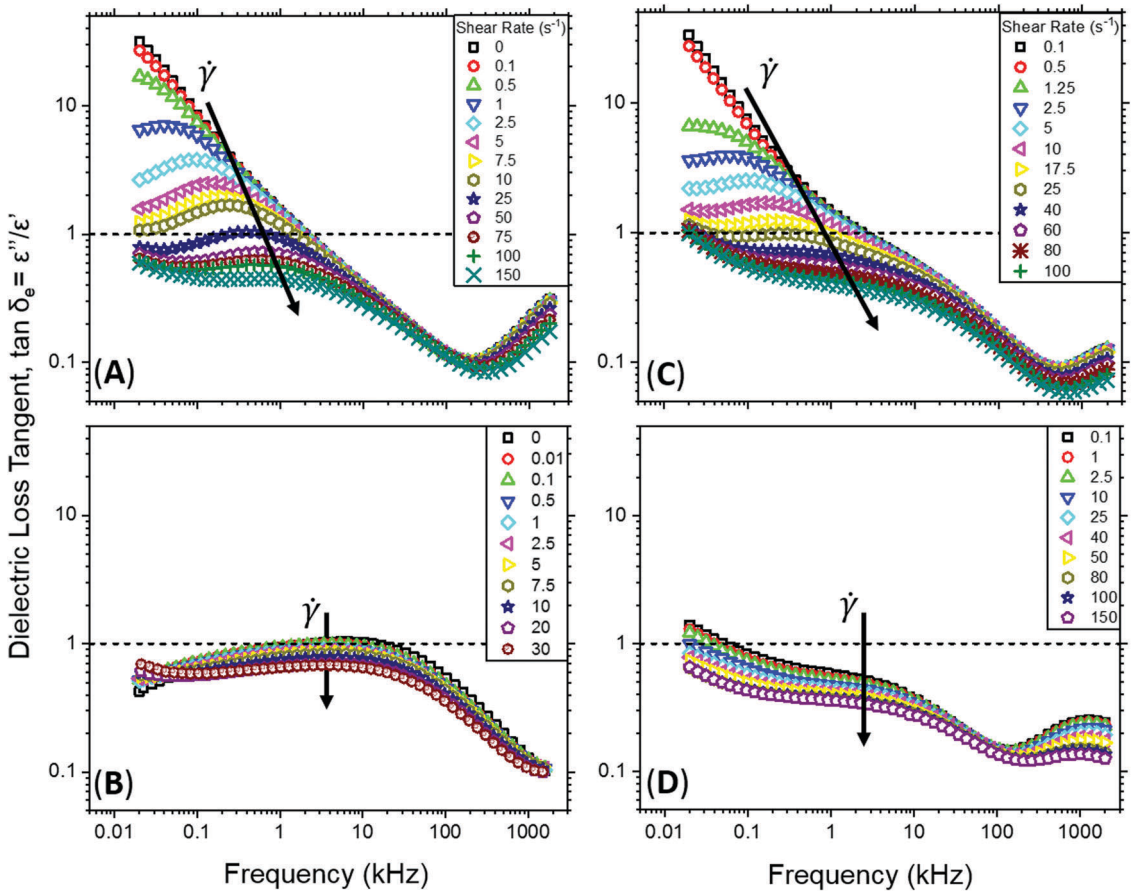

Fig. 4 Dielectric loss tangent as a function of shear rate for (A) branched WLMs in decane ($W = 2.8$, $C_{LEC} = 75$ mg mL^{-1}) (B) linear WLMs in cyclohexane ($W = 10$, $C_{LEC} = 75$ mg mL^{-1}), (C) branched WLMs in decane ($W = 2.8$, $C_{LEC} = 50$ mg mL^{-1}), (D) unbranched WLMs in decane ($W = 2.4$, $C_{LEC} = 50$ mg mL^{-1}).

If the WLMs are disconnected, they should be highly resistive and exhibit low dielectric loss. In contrast, the branched WLMs in decane have $\tan\delta_e > 1$ in the LF region at rest and under slow flow, but develop a peak whose position shifts to higher frequencies and whose magnitude drops below $\tan\delta_e = 1$ at higher shear rates. This crossover behavior is consistent with branch breaking and seemingly provides a convenient metric for quantifying the shear rate required to break most system-spanning branch connections. For branched WLM samples, we can define a critical disconnection shear rate, $\dot{\gamma}_{dis}$, based on the loss tangent crossover. For the 50 mg mL^{-1} branched WLMs in decane ($W = 2.8$, Fig. 4c) $\dot{\gamma}_{dis} \approx 25$ s^{-1}, below which the micelles maintain branch points and above which they appear dielectrically similar to the un-branched micelles ($W = 2.4$, Fig. 4d). It is notable that these details are resolved *via* flow-dielectric measurements and do not require a prior knowledge of the stress response and rheology; however, rheological and SANS measurements are necessary to link features in the dielectric spectra with macroscopic stress and microstructural anisotropy.

Dielectric RheoSANS: branched *vs.* unbranched WLMs in decane

Having established some basics of the dielectric response of reverse WLMs under flow, simultaneous measurements of the dielectric spectra with both the stress and microstructure are performed to investigate the flow behavior of these varying topologies. First, results for unbranched and branched WLMs in decane at equivalent lecithin concentrations are compared. Fig. 5 and 6 summarize dielectric RheoSANS experiments on unbranched and branched reverse WLMs undergoing steady-shear flow. After reaching a steady-state stress, both 2D SANS scattering patterns and dielectric frequency sweeps were collected. SANS measurements in the flow-vorticity (1–3) plane of shear are used to quantify segmental anisotropy at select shear rates prior to and along the stress plateau. As discussed earlier the AC conductivity contains information about the transport of ions across the gap, making it sensitive to static and dynamic network connectivity and anisotropy. On the other hand, the AC permittivity contains information pertaining to the collective arrangement and dynamics of dipoles in the system. The microstructural origin of such dipoles in the reverse WLM system is tied to both polymer chain dynamics[47] and Maxwell–Wagner type interfacial polarization[31] arising at the water/headgroup/oil interface. The shear-rate dependence of such processes are separated, as will be discuss later on.

Flow curves for both branched and unbranched WLMs display strong shear-thinning rheology and stress plateaus characteristic of semi-dilute WLMs. The differences in zero-shear viscosity and primary relaxation time discussed earlier

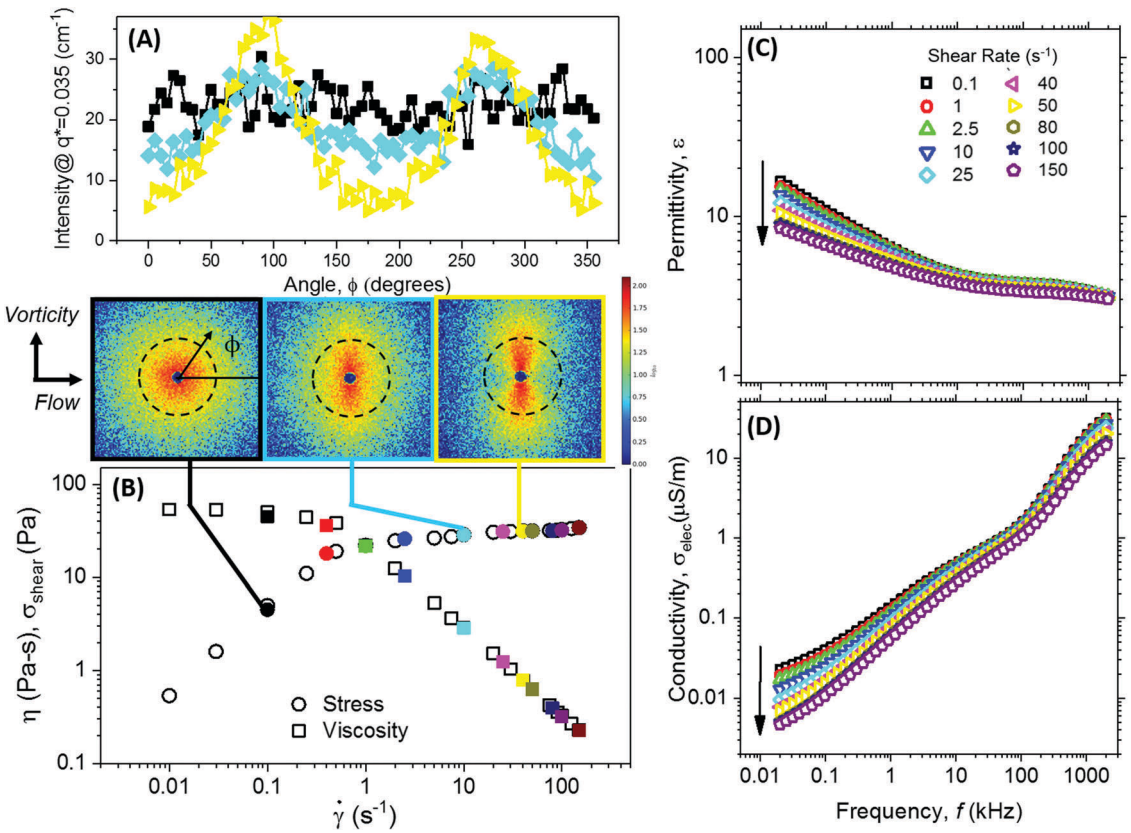

Fig. 5 Dielectric RheoSANS on un-branched reverse WLMs in deuterated *n*-decane. Lecithin concentration is 50 mg mL^{-1} and the molar ratio of water to surfactant is $W = 2.4$. (A) Representative 2D SANS patterns in the 1–3 plane and 1D annular average profiles used to quantify anisotropy *via* an alignment factor. (B) Steady-shear flow sweep measured in independent experiments. Open symbols are obtained offline and filled symbols are shear rates measured during dielectric RheoSANS. (C) Frequency-dependent permittivity and (D) conductivity spectra measured at steady-state as a function of shear rate.

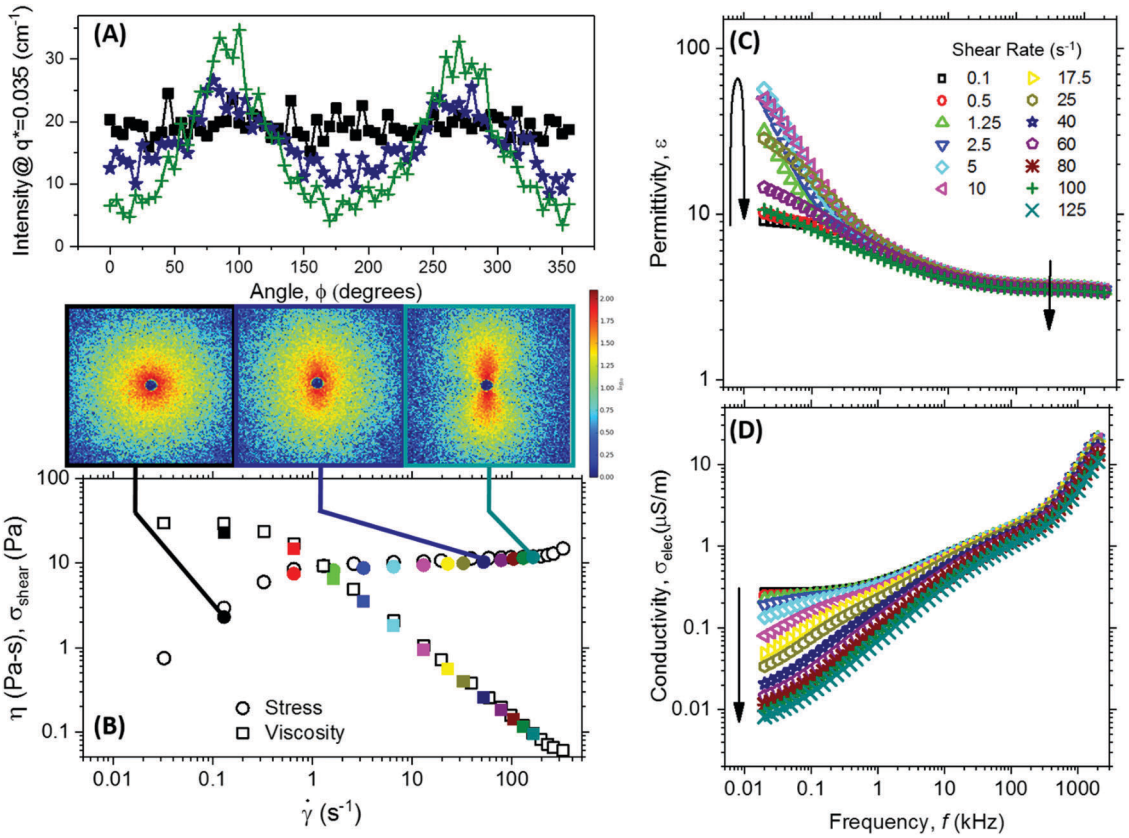

Fig. 6 Dielectric RheoSANS on branched reverse WLMs in deuterated *n*-decane. Lecithin concentration is 50 mg mL^{-1} and the molar ratio of water to surfactant is W = 2.8. (A) Representative 2D SANS patterns in the 1–3 plane and 1D annular average profiles used to quantify anisotropy *via* a 1–3 alignment factor. (B) Steady-shear flow sweep measured in independent experiments. Open symbols are obtained offline and filled symbols are shear rates measured during dielectric RheoSANS. (C) Frequency-dependent permittivity and (D) conductivity spectra measured at steady-state as a function of shear rate. Select shear rates are shown in (C) for clarity.

are reflected in the steady-shear flow curves. 2D SANS patterns at the segmental length scale both display diffuse scattering expected for polydisperse WLMs.[22] SANS patterns are isotropic at rest and at low shear rates, and visible anisotropy develops in the 1–3 plane as shear rate increases along the stress plateau. This is attributable to alignment of locally cylindrical segments of the worm-like chains. Annular averages of the 2D SANS patterns capture this anisotropy as intensity peaks at angles of 90° and 270° relative to the flow direction. There is no signifiable difference in the 2D patterns and annular average profiles between the branched and unbranched micelles, reflecting the subtle microstructural changes that occur as topology evolves relative to the structure factor effects of intermicellar interactions associated with entanglement. In contrast to the rheological and microstructural signals, we know from discussion of Fig. 4 that the electrical properties under shear are sensitive to topology. For the unbranched micelles in Fig. 5, both the conductivity and permittivity undergo weak monotonic decreases in response to shear. The qualitative frequency dependence of both the permittivity and conductivity is preserved for the unbranched micelles under shear. This behavior is consistent with rheo-dielectric measurements of entangled linear polymer chains in strong shear flow,[48] although there is an additional contribution to the stress response in this work from micelle breakup under flow.

Meanwhile, the electrical properties of the branched micelles in Fig. 6 undergo striking change under shear. Fig. 6c shows that the conductivity plateau/DC conductivity disappears and the conductivity drops precipitously (≈2 orders of magnitude) with increasing shear rate. The conductivity decrease with increasing shear is directly related to changes in charge transport in the water-swollen micelle cores and is coupled to micelle breakup and reformation and the number of sample-spanning branch/junction point connections in the 1–3 plane. Further, the low-frequency permittivity of the branched WLMs undergoes a non-monotonic change in response to shear while the high-frequencies permittivity monotonically decreases in response to shear. The low-frequency permittivity initially increases with shear rate, then reaches a maximum at intermediate shear rates, and steadily decreases at higher shear rates. As the low-frequency permittivity has been associated with rotational motion of the micelles,[49] this non-monotonic behavior must reflect the competition between breaking of system-spanning, percolated branch points, which frees the micelles to rotate, and flow-alignment, which restricts micelle rotation. These results are in qualitative agreement with temperature-dependent dielectric measurements of branched WLMs in isooctane,[41] where it is observed that the LF permittivity increases and LF conductivity decreases upon heating over a modest range (18 °C to 30 °C),

reflecting the breaking of branch points prior to large-scale length changes at higher temperatures (30 °C to 50 °C).

Select features of the dielectric RheoSANS data in Fig. 5 and 6 are plotted in Fig. 7 to compare correlations between the permittivity, conductivity, viscosity, and alignment for the branched and unbranched WLMs. Steady-shear electrical, rheological, and alignment data are presented in Fig. 7 as a function of Weissenberg number $Wi = \tau_R\dot{\gamma}$. Notably, the onset of shear thinning is shifted to smaller Wi for the branched WLMs compared with the unbranched WLMs. Simultaneously, there is no significant difference in 1–3 alignment factor between branched and unbranched WLMs over the range of measured Weissenberg numbers. Careful inspection of the curves suggests that the alignment factor for the unbranched micelles is slightly higher than the branched micelles at a given Weissenberg number, and that the unbranched micelles develop distinguishable anisotropy ($A_f = 0.06$) above the noise level ($A_f = 0.03$) at $Wi \approx 3$ while the branched micelles do not obtain such a level of anisotropy until $Wi \approx 13$. Interestingly, this range of Weissenberg numbers corresponds to the region of greatest interest with respect to the dielectric properties. The low-frequency permittivity of the branched micelles increases by a factor of 8 and the conductivity by a factor of 2 in this low-to-intermediate Wi region prior to alignment. Above $Wi \approx 15$ the permittivity begins to decrease and the conductivity begins to thin more strongly with increasing shear rate. At high shear rates, the conductivity, permittivity, alignment factor, and viscosity of the branched micelles all exhibit scaling with $\sim Wi^{-1}$. The unbranched micelles exhibit dielectric properties that correlate directly with alignment at all shear rates, suggesting that flow of these WLMs is always dominated by the release of segments from constrained entanglements and their subsequent alignment with the flow. In the reverse WLMs investigated here, both the dielectric and SANS measurements appear to successfully measure anisotropy in the 1–3 plane at high shear rates.

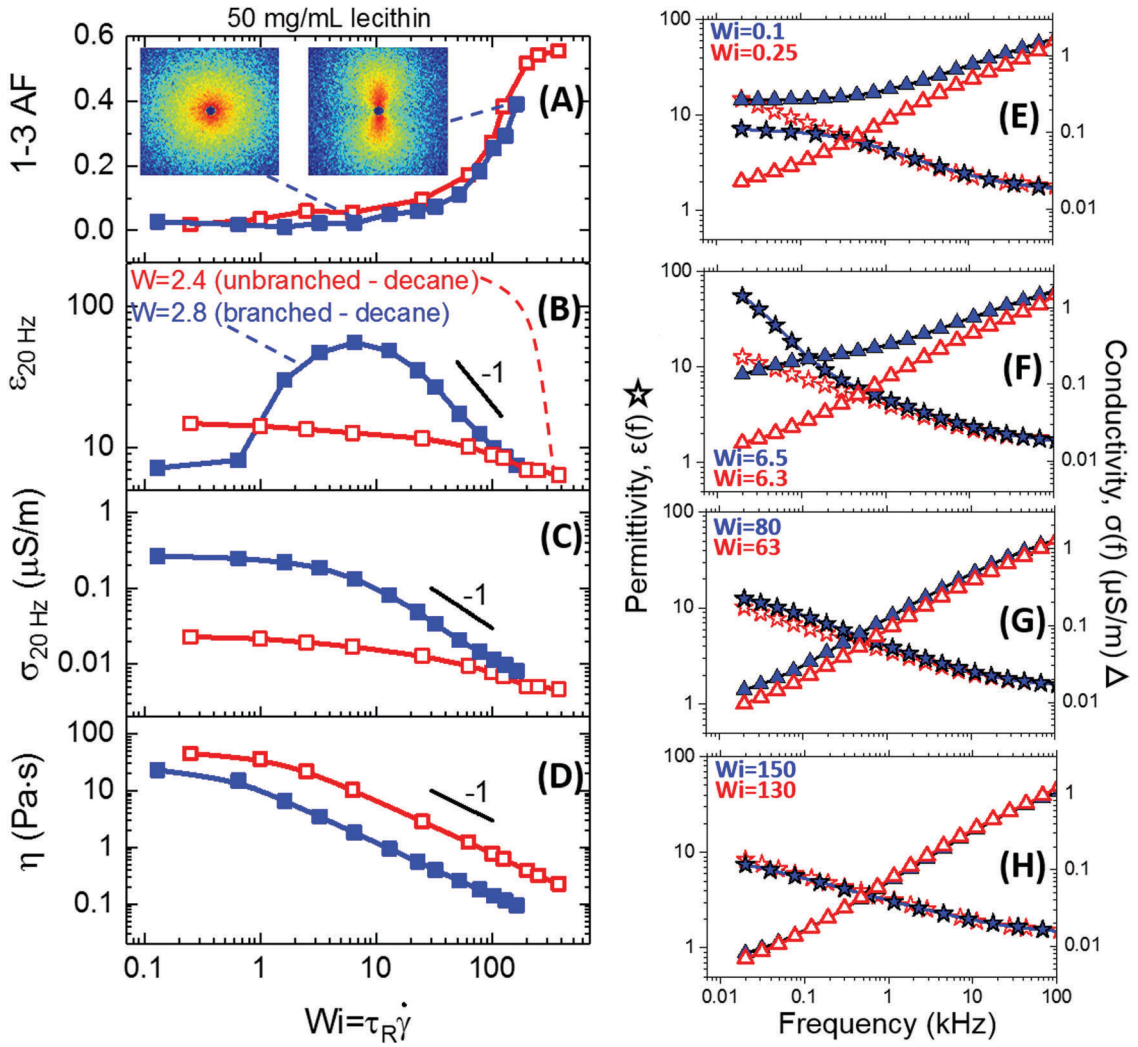

Fig. 7 Dielectric RheoSANS of WLMs in decane: branched (closed blue symbols) and unbranched (open red symbols). (A) 1–3 alignment factor at segmental length scale including representative 2D SANS patterns of the branched micelles, (B) low-frequency permittivity and (C) conductivity, and (D) viscosity as a function of Weissenberg number. Lines connecting the data are drawn to guide the eye. Power law slopes highlight anisotropy-driven correlations at high shear rates. (E–H) Dielectric spectra capturing the low-frequency relaxation under shear rates producing approximately equal extents of alignment: permittivity (stars) and conductivity (triangles). The curves largely overlay under the strong shear rates in panel H.

These correlations between dielectric properties, stress, and alignment is reminiscent of the flow-birefringence for polymer solutions,[50] the stress-SANS rule for viscoelastic WLMs,[51] and similar stress-dielectric formalisms used to describe polymeric systems.[52]

Comparing the dielectric spectra of branched and unbranched WLMs at equivalent degrees of alignment in Fig. 7 reinforces our picture of branched WLM flow relative to unbranched WLMs. The difference in AC response at low-to-moderate flows is attributable to branching and the breakup of labile, system-spanning branch points that are absent in the unbranched sample. Under strong flows the AC dielectric response of the two WLMs begins to converge as most branched points are released and the WLMs are moderately aligned. Finally, at very large Weissenberg numbers the micelles are strongly aligned and sufficiently broken that the AC dielectric responses practically overlay. At these high shear rates where the spectra overlap, the dielectric and microstructural measurements for both branched and unbranched WLMs reflect the same anisotropy in the 1–3 plane.

To summarize this section, Dielectric RheoSANS measurements have uniquely identified two regimes of flow for branched WLMs micelles: (1) branch breaking at low-to-intermediate shear rates followed by (2) alignment-driven anisotropy at high shear rates. These findings provide the most conclusive evidence to date that WLMs first relieve stress under flow by branch breaking, resulting in an earlier onset of shear thinning than is observed for unbranched WLMs whose shear thinning is solely attributable to entanglement anisotropy.

Dielectric RheoSANS: branched WLMs in decane *vs.* linear WLMs in cyclohexane

We have also performed dielectric RheoSANS experiments which compare purely linear WLMs in cyclohexane to branched WLMs in decane. In this case, the surfactant concentrations are 75 mg mL^{-1} which is higher than the 50 mg mL^{-1} samples discussed in the previous section. Again, it is important to emphasize that the WLMs in decane and cyclohexane differ not only in topology but also in breakage kinetics. In decane, the minimum in loss modulus for the WLMs in Fig. 2 suggest breakage times $\approx$0.1 seconds. If the decane WLMs obey fast-breakage kinetics, then the observed primary relaxation time is the geometric mean of the breakage time and the reptation time,[5] $\tau_R = (\tau_{break}\tau_{rep})^{1/2}$. This results in estimated reptation times on the order of 60 seconds. Meanwhile, the measured breakup times for cyclohexane WLMs have been reported to be on the order of minutes and are of the same magnitude as the reptation time for the linear WLMs.[26]

Select features of the dielectric RheoSANS experiments are plotted in Fig. 8. The two WLM systems display similar zero-shear viscosities with similar shear-thinning power law exponents, as evidenced in Fig. 5; however, they exhibit drastically different alignment and dielectric properties in response to shear over a comparable range of Weissenberg numbers. The alignment factor data for the linear WLMs shows weak alignment and an apparent alignment plateau at intermediate Weissenberg numbers. This is indicative of strong shear banding which has been reported for linear lecithin WLMs in deuterated cyclohexane *via* rheo-NMR and velocimetry.[53] Our RheoSANS data supports a picture of shear banding in the linear WLMs as the 2D SANS patterns at higher Weissenberg numbers (inset, Fig. 8A) suggest a coexistence between isotropic, un-aligned micelles and anisotropic, strongly aligned micelles. This coexistence is smeared in the 1–3 plane of shear, and appears in the 2D SANS patterns as an isotropic halo superimposed over an anisotropic stripe.[54] In the presence of shear banding, the gap-average dielectric properties reflect this same smeared phase coexistence. This prominent signature of shear banding in the SANS patterns is not observed for the branched WLMs in decane, where the anisotropic SANS patterns (inset, Fig. 8A) appear homogeneously aligned much like the WLMs in Fig. 5 and 6. It has been suggested that moderate degrees of branching may suppress shear banding in aqueous WLMs;[19] however, we have pointed out that in this work both

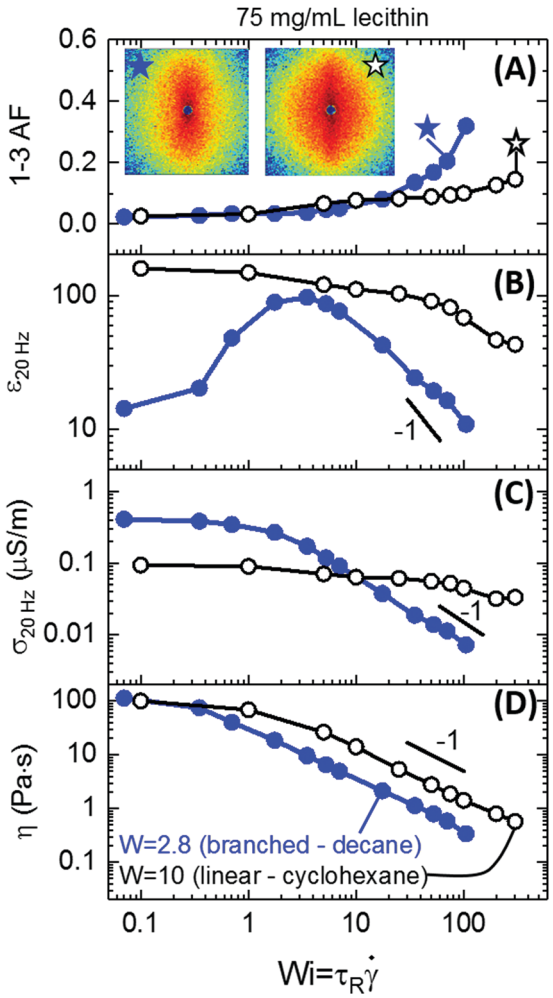

Fig. 8 Comparison of simultaneous dielectric RheoSANS data for branched WLMs in decane (closed symbols) *vs.* linear WLMs in cyclohexane (open symbols). (A) 1–3 alignment factor at segmental length scale including representative anisotropic SANS patterns of the branched and linear WLMs, low-frequency (B) permittivity and (C) conductivity from dielectric spectroscopy, and (D) viscosity as a function of Weissenberg number, or normalized shear rate.

the topology and breakage kinetics are different between the two solvent systems. We have not made efforts to quantify shear banding or spatial flow heterogeneity in this work, but our 1–3 plane SANS measurements suggest that the gap-average alignment of the branched WLMs is significantly more uniform than the linear WLMs in cyclohexane. As such, we will limit our commentary on the dielectric behavior of the linear WLMs under flow to the following: the linear WLMs exhibit subtle decreases in gap-average conductivity and permittivity over all shear rates that correlates with an increase in gap-average structural anisotropy. This is qualitatively consistent with the behavior of the unbranched WLMs in decane.

The dielectric RheoSANS results for the 75 mg mL^{-1} branched micelles in decane are consistent with the trends for 50 mg mL^{-1} discussed in Fig. 6 and 7. At low to moderate Weissenberg numbers (Wi $\leq$ 10) the viscosity decreases approximately one order of magnitude with little to no observable increase in 1–3 alignment factor. Again, the low-frequency (20 Hz) dielectric properties of the branched WLMs exhibit notable changes with increasing shear rate prior to chain alignment: permittivity increases by a factor of 7 before beginning the initial descent while conductivity decreases by a factor of 4. The permittivity increase reflects an increased dielectric strength $\Delta\varepsilon$ of the low-frequency relaxation, which we attribute to the release of branch points and increasing rotational mobility the micelles. Effectively, the number of dipoles free to rotate in the system increases as branches are broken. The conductivity decrease is tied directly to the breaking of percolated pathways that span the gap. Both the 50 mg mL^{-1} and 75 mg mL^{-1} branched WLMs in decane undergo shear thinning at Weissenberg numbers less than 1, further evidence that branching plays a critical role in the early stage of the stress plateau, followed by alignment-driven anisotropy at higher shear rates reflected in both the dielectric and SANS measurements. These results further demonstrate how dielectric RheoSANS provides an unprecedentedly clear picture for the flow of reverse WLMs. It is important to reiterate that dielectric RheoSANS only provides structural and dielectric anisotropy in the 1–3 plane of shear, and that this work does not address flow-induced structure that develops in the other planes of shear. WLMs are known to orient at an angle with the flow direction which is only resolvable with 1–2 plane measurements,[51] and this orientation may contribute to the formation or dislocation of conductive pathways across the gap. While notable, fully characterization of structural and dielectric anisotropy lies outside the scope of the current study.

Correlations between the high-frequency dielectric properties and alignment

Until this point, we have primarily discussed the low-frequency dielectric properties because they are sensitive to branching and micelle dynamics. Based on the loss tangent plots in Fig. 3, we know that the WLMs in decane also exhibit a high-frequency dielectric relaxation which is sensitive to the amount of solubilized water in the core. We hypothesize that the high frequency dielectric relaxation resolved in the decane reverse micelles is of the Maxwell–Wagner–Sillars interfacial polarization type[55] arising from dielectric contrast between the oil/alkane tails and the water/zwitterionic headgroups in the micelle core. This interfacial polarization importantly depends on particle alignment of the dispersed phase relative to the applied electric field,[31] and decreases in permittivity and conductivity are expected as micelles are aligned in the plane perpendicular to the oscillating electric field. The anisotropy-driven effect is shown in Fig. 9, where the normalized change in high-frequency conductivity and permittivity is plotted parametrically against normalized alignment factor. The expected correlation between increases in alignment and decreases in the high-frequency dielectric properties are observed for both samples, however the same normalization cannot be made for the branched WLMs because the samples were sheared at high enough Weissenberg numbers to reach an alignment maximum plateau. The dielectric and SANS measurements are both made in the 1–3 plane, and both the SANS contrast and dielectric contrast arises from the surfactant + water core regions of the sample. The ability to track both alignment through the high-frequency dielectric properties shown in Fig. 9 and branching through the low-frequency dielectric properties discussed earlier provides the strong microstructural basis for interpreting rheo-dielectric measurements in the absence of SANS. Direct alignment correlations across all dielectric frequencies for the unbranched micelles will prove useful in fingerprinting transient anisotropy during fast transient flows such as startup and large-amplitude oscillatory shear *via* purely rheo-dielectric measurements.

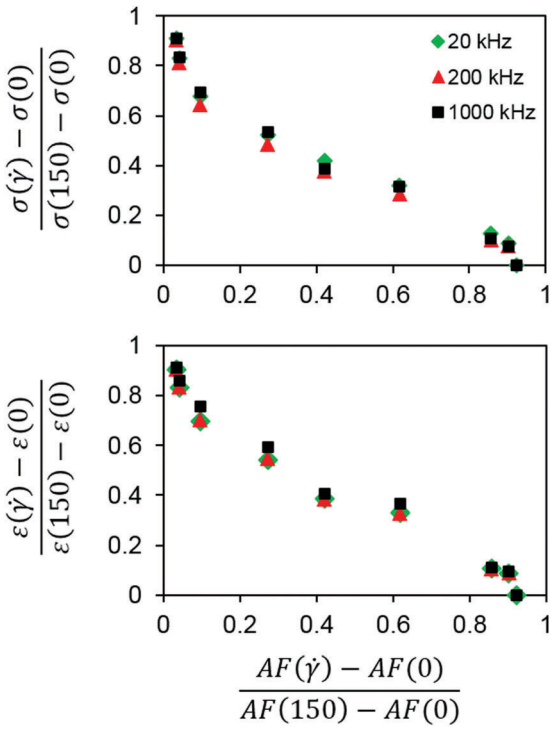

Fig. 9 High-frequency conductivity and permittivity as a function of 1–3 plane alignment factor for unbranched WLMs in decane at three different frequencies. The conductivity and permittivity at rest is subtracted from the value under shear and normalized by the difference between the shear rate for maximum alignment (150 s^{-1}) and at rest values.

Conclusions

Structure–property relationships for the steady-shear flow behavior of water-swollen lecithin reverse worm-like micelles have been determined using a combination of rheology, small-angle neutron scattering, and dielectric spectroscopy. Three WLM systems with distinguishable topologies (branched or non-branched) and recombination dynamics (fast or slow micelle breakage times) were identified based on their dielectric properties at rest and under flow. The gap-average low-frequency permittivity of the WLM solutions provided a unique fingerprint of branching as the permittivity increased at low-to-moderate shear rates, when system-spanning connectivity is present, prior to strong decreases in permittivity at higher shear rates. The permittivity and conductivity only decrease in response to flow for WLMs that did not exhibit branching. A novel dielectric RheoSANS technique independently distinguishes changes in global network connectivity from structural anisotropy that develops as reverse WLMs align in the flow field. Our findings indicate that branched WLMs first relieve stress by releasing branch points along system-spanning percolated micelle pathways, after which the branched-but-broken aggregates orient with the flow. In contrast, the flow-dielectric properties of non-branched WLMs can be attributed predominantly to structural anisotropy. The dielectric RheoSANS comparison of branched and unbranched WLMs in decane provides convincing evidence that topology, when properly isolated from strong intermicellar repulsions and in the absence of significant flow instabilities such as shear-banding, has a subtle but noticeable effect of shifting the onset of shear thinning of the WLMs to lower effective Weissenberg numbers. By identifying the microstructural origins of features in the broadband dielectric spectra in this work, we have paved the way for future rheo-dielectric characterization of lecithin/water/oil reverse WLMs undergoing more complex transient flows useful for testing microstructure-based constitutive models of WLM rheology.

Disclaimer

Certain commercial equipment, instruments, or materials are identified in this paper to specify the experimental procedure adequately. Such identification is not intended to imply recommendation or endorsement by the National Institute of Standards and Technology, nor is it intended to imply that the materials or equipment identified are necessarily the best available for the purpose. Unless otherwise specified, error bars are one standard deviation from the mean.

Conflicts of interest

There are no conflicts to declare.

Acknowledgements

The authors would like to acknowledge the NIST Center for Neutron Research CNS grant for partial funding during this time. J. K. R. acknowledges support from a National Research Council Research Associates Program. N. J. W. acknowledges support under cooperative agreements #70NANB12H239, 70NANB15H260, and 70NANB17H302 from NIST, U.S. Department of Commerce.

References

1 *Giant micelles: properties and applications*, ed. R. Zana and E. W. Kaler, CRC Press (Taylor and Francis), Boca Raton, 2007.
2 C. A. Dreiss, *Soft Matter*, 2007, **3**, 956.
3 G. Palazzo, *Soft Matter*, 2013, **9**, 10668.
4 M. E. Cates, *Macromolecules*, 1987, **20**, 2289–2296.
5 M. E. Cates and S. J. Candau, *J. Phys.: Condens. Matter*, 1990, **2**, 6869–6892.
6 G. Ovarlez, S. Rodts, X. Chateau and P. Coussot, *Rheol. Acta*, 2009, **48**, 831–844.
7 B. A. Schubert, N. J. Wagner, E. W. Kaler and S. R. Raghavan, *Langmuir*, 2004, **20**, 3564–3573.
8 T. J. Drye and M. E. Cates, *J. Chem. Phys.*, 1992, **96**, 1367–1375.
9 P. A. Vasquez, G. H. McKinley and L. Pamela Cook, *J. Nonnewton. Fluid Mech.*, 2007, **144**, 122–139.
10 M. W. Liberatore, F. Nettesheim, P. A. Vasquez, M. E. Helgeson, N. J. Wagner, E. W. Kaler, L. P. Cook, L. Porcar and Y. T. Hu, *J. Rheol.*, 2009, **53**, 441–458.
11 C. Lepper, P. J. B. Edwards, R. Dykstra and M. A. K. Williams, *Soft Matter*, 2011, **7**, 10291.
12 S. Kim, J. Mewis, C. Clasen and J. Vermant, *Rheol. Acta*, 2013, **52**, 727–740.
13 S. A. Rogers, M. A. Calabrese and N. J. Wagner, *Curr. Opin. Colloid Interface Sci.*, 2014, **19**, 530–535.
14 N. Dan and S. A. Safran, *Adv. Colloid Interface Sci.*, 2006, **123–126**, 323–331.
15 F. Lequeux, *Europhys. Lett.*, 1992, **19**, 675–681.
16 Y. I. González and E. W. Kaler, *Curr. Opin. Colloid Interface Sci.*, 2005, **10**, 256–260.
17 K. Vogtt, G. Beaucage, M. Weaver and H. Jiang, *Langmuir*, 2015, **31**, 8228–8234.
18 W. Chen, P. D. Butler and L. J. Magid, *Langmuir*, 2006, **23**, 6539–6548.
19 M. A. Calabrese, S. A. Rogers, R. P. Murphy and N. J. Wagner, *J. Rheol.*, 2015, **59**, 1299–1328.
20 R. Scartazzini and P. L. Luisi, *J. Phys. Chem.*, 1988, **92**, 829–833.
21 P. Schurtenberger, G. Jerke, C. Cavaco and J. S. Pedersen, *Langmuir*, 1996, 2433–2440.
22 G. Jerke, J. Pedersen, S. Egelhaaf and P. Schurtenberger, *Phys. Rev. E: Stat. Phys., Plasmas, Fluids, Relat. Interdiscip. Top.*, 1997, **56**, 5772–5788.
23 P. A. Cirkel and G. J. M. Koper, *Langmuir*, 1998, **14**, 7095–7103.
24 Y. A. Shchipunov, *Colloids Surf., A*, 2001, **183–185**, 541–554.
25 S.-H. Tung, Y.-E. Huang and S. R. Raghavan, *Langmuir*, 2007, **23**, 372–376.
26 U. Olsson, J. Börjesson, R. Angelico, A. Ceglie and G. Palazzo, *Soft Matter*, 2010, **6**, 1769.
27 P. Schurtenberger, L. J. Magid, J. Penfold and R. Heenan, *Langmuir*, 1990, **6**, 1800–1803.

28 R. Angelico, U. Olsson, K. Mortensen, L. Ambrosone, G. Palazzo and A. Ceglie, *J. Phys. Chem. B*, 2002, **106**, 2426–2428.
29 R. Angelico, C. O. Rossi, L. Ambrosone, G. Palazzo, K. Mortensen and U. Olsson, *Phys. Chem. Chem. Phys.*, 2010, **12**, 8856–8862.
30 R. Angelico, A. Ceglie, G. Colafemmina, F. Delfine, U. Olsson and G. Palazzo, *Langmuir*, 2004, **20**, 619–631.
31 K. Asami, *Prog. Polym. Sci.*, 2002, **27**, 1617–1659.
32 S. H. Chen, J. Rouch, F. Sciortino and P. Tartaglia, *J. Phys.: Condens. Matter*, 1999, **6**, 10855–10883.
33 S. Schrodle, R. Buchner and W. Kunz, *ChemPhysChem*, 2005, **6**, 1051–1055.
34 P. Cirkel, J. van der Ploeg and G. Koper, *Phys. Rev. E: Stat. Phys., Plasmas, Fluids, Relat. Interdiscip. Top.*, 1998, **57**, 6875–6883.
35 J. J. Richards, C. V. L. Gagnon, J. R. Krzywon, N. J. Wagner and P. D. Butler, *J. Visualized Exp.*, 2017, **122**, e55318.
36 J. J. Richards, N. J. Wagner and P. D. Butler, *Rev. Sci. Instrum.*, 2017, **88**, 105115.
37 *Broadband Dielectric Spectroscopy*, ed. F. Kremer and A. Schönhals, Springer Berlin Heidelberg, Berlin, Heidelberg, 2003.
38 C. J. Glinka, J. G. Barker, B. Hammouda, S. Krueger, J. J. Moyer and W. J. Orts, *J. Appl. Crystallogr.*, 1998, **31**, 430–445.
39 S. R. Kline, *J. Appl. Crystallogr.*, 2006, **39**, 895–900.
40 L. M. Walker and N. J. Wagner, *Macromolecules*, 1996, **29**, 2298–2301.
41 P. A. Cirkel, M. Fontana and G. J. M. Koper, *J. Dispersion Sci. Technol.*, 2001, **22**, 211–219.
42 R. Angelico, S. Amin, M. Monduzzi, S. Murgia, U. Olsson and G. Palazzo, *Soft Matter*, 2012, **8**, 10941.
43 A. G. Zilman and S. A. Safran, *Phys. Rev. E: Stat., Nonlinear, Soft Matter Phys.*, 2002, **66**, 1–28.
44 R. Angelico, G. Palazzo, G. Colafemmina, P. A. Cirkel, M. Giustini and A. Ceglie, *J. Phys. Chem. B*, 1998, **102**, 2883–2889.
45 I. Martiel, L. Sagalowicz and R. Mezzenga, *Langmuir*, 2014, **30**, 10751–10759.
46 A. V. Shibaev, V. S. Molchanov and O. E. Philippova, *J. Phys. Chem. B*, 2015, **119**, 15938–15946.
47 W. H. Stockmayer, *Pure Appl. Chem.*, 1967, **15**, 539–554.
48 H. Watanabe, S. Ishida and Y. Matsumiya, *Macromolecules*, 2002, **35**, 8802–8818.
49 P. Cirkel, J. van der Ploeg and G. Koper, *Phys. Rev. E: Stat. Phys., Plasmas, Fluids, Relat. Interdiscip. Top.*, 1998, **57**, 6875–6883.
50 G. G. Fuller and L. G. Leal, *J. Polym. Sci., Polym. Phys. Ed.*, 1981, **19**, 557–587.
51 M. E. Helgeson, P. A. Vasquez, E. W. Kaler and N. J. Wagner, *J. Rheol.*, 2009, **53**, 727.
52 Y. Peng, Y. M. Shkel and G. Kim, *J. Rheol.*, 2005, **49**, 297.
53 R. Angelico, L. Gentile, G. A. Ranieri and C. Oliviero Rossi, *RSC Adv.*, 2016, **6**, 33339–33347.
54 J.-F. Berret, D. C. Roux and P. Lindner, *Eur. Phys. J. B*, 1998, **5**, 67–77.
55 T. Hanai, *Kolloid-Z.*, 1960, **171**, 23–31.